(Received 31 January 2024, Accepted 9 March 2024, Scheduled 20 March 2024)

Compact Dual-Polarized Antenna with Wide Band and High Isolation Using Characteristic Mode Analysis

Zhongjie Zhan, Wen Huang*, Rui Deng, and Bao Li

School of Optoelectronic Engineering, Chongqing University of Posts and Telecommunications, Chongqing 400065, China

ABSTRACT: In this paper, a compact dual-polarized antenna with wide band and high isolation is proposed, which can be applied to the 5G WiFi frequency band. The antenna is composed of 2×2 arrayed patches and two orthogonal L-shaped probe structures with reduced middle patch width and loaded U-shaped slots. The proposed antenna achieves a compact size by eliminating the need for a complex feeding network, instead utilizing only two closely spaced L-shaped probes for feeding. The antenna's radiation modes excited by two ports are orthogonal in polarization direction, and each port can excite two linearly polarized radiation modes respectively within the operating frequency band, thereby achieving dual-linear polarization and wideband performance. The antenna is analyzed and designed using characteristic mode analysis (CMA). By reducing the patch middle width and loading U-shaped slots on the L-shaped probe of the antenna, the suppression of high-order modes, improvement of isolation, and reduction of cross-polarization levels are achieved. The size of the antenna is $0.54\lambda_0 \times 0.54\lambda_0 \times 0.068\lambda_0$ (λ_0 is the free-space wavelength of central frequency). The measured bandwidth is 23.5% (4.73 GHz–5.99 GHz) with $|S_{11}| < -10$ dB, $|S_{21}| < -27.9$ dB, boresight gain of 4.8 dBi–6.2 dBi, and cross-polarization levels better than -23 dB.

1. INTRODUCTION

Dual-polarized antennas offer a pair of communication channels with the same operating frequency but orthogonal polarization, enabling frequency reuse and polarization diversity. They have significant advantages such as high signal transmission capacity and strong anti-multipath fading [1–6], making them widely used in mobile communication systems. With the rapid development of modern RF front-end technology, there is a growing demand for dual-polarized antenna integration with increasingly limited space available for antenna design. Microstrip dual-polarized antennas have gained significant attention for their small sizes, light weights, low costs, and ease of integration with circuits. However, it is still challenging to achieve a compact wideband dual-polarized microstrip antenna while considering the good impedance bandwidth, high isolation, and high front-to-back ratios (FBRs).

Multiple approaches have been reported for achieving wideband dual-polarized antennas with high port isolation. For example, through aperture slots feed, using two [7–9] or four [10] feeding microstrip lines to excite linearly polarized radiation modes from the metasurface and the aperture slot can result in a wideband dual-polarized metasurface antenna with high isolation. However, the aperture slot feeding method may lead to low FBRs. Other approaches involve using four L-shaped probes [11, 12] or other similar probe structures [13, 14], combined with a feeding network that provides a 180° phase shift and power division function. These methods can realize wideband dual-polarized microstrip antennas with high isolation and low cross-polarization levels. However, the feeding network not only introduces additional losses but also increases the sizes of the antennas.

Several research methods have been proposed to achieve high-isolation dual-polarized microstrip antennas with compact sizes. In [15], a cross-slot antenna with a size of only $0.293\lambda_0 \times 0.293\lambda_0 \times 0.008\lambda_0$ is presented, which achieves a high isolation but with a narrow bandwidth and poor directionality. Exciting the patch radiation modes with two probes can realize high isolation, high FBRs, and compact sizes, but the antenna bandwidth is narrow [16, 17]. In [18], by exciting two-layer E-shaped patches with two probes, the antenna has a port isolation more than 30 dB and a stable gain, but the operating bandwidth is only 7.7%. Using a structure with two L-shaped probes and rectangular patches can achieve wide bandwidths, high FBRs, and compact antenna sizes [11, 19]. However, the antennas exhibit unsatisfactory isolations and cross-polarization levels performance.

In this paper, a compact wideband high-isolation dual-polarized antenna is proposed. The antenna consists of 2×2 arrayed patches and two L-shaped probes with reduced middle patch width and U-shaped slots. The L-shaped probe structures and patches structure are adopted in the antenna design, without using complex feeding networks, to achieve a compact antenna size. Using the CMA to design the antenna, the patch middle is reduced, which suppresses high-order modes and improves the isolation of the antenna. Furthermore, U-shaped slots are etched on the L-shaped probe to provide high isolation characteristics for the antenna. The measurements show that a good performance is achieved in the frequency range of 4.73–5.99 GHz, with high port isolation, high FBRs, and low cross-polarization level.

* Corresponding author: Wen Huang (huangwen@cqupt.edu.cn).

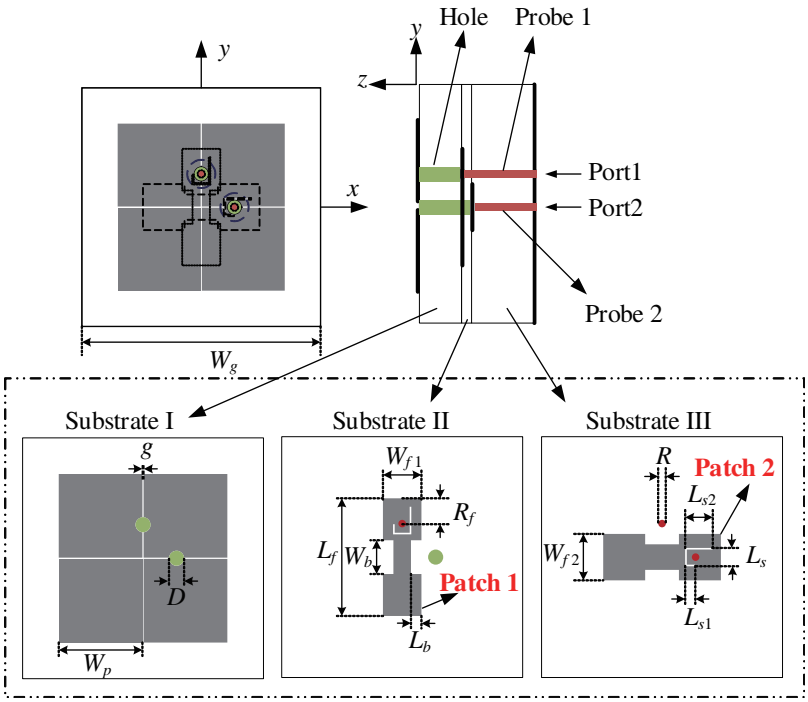

FIGURE 1. Configuration of the proposed antenna.

TABLE 1. Dimensions of the proposed antenna.

Parameters	Value	Parameters	Value	Parameters	Value
W_g	30.0 mm	g	0.15 mm	W_p	10.4 mm
D	1.9 mm	L_f	14.7 mm	W_b	4.2 mm
W_{f1}	4.8 mm	L_s	2.3 mm	L_b	1.3 mm
R	0.94 mm	W_{f2}	5.8 mm	L_{s1}	1.3mm
L_{s2}	3.4mm	R_f	3.15 mm		

2. DESIGN OF ANTENNA

2.1. Antenna Structure

Figure 1 shows the geometry of the antenna and top views of the employed substrates. In the antenna design, three layers of F4B substrate are used all with $\varepsilon_r = 2.65$ and $\tan\sigma = 0.0015$. The thickness of substrate I is 1.5 mm; the thickness of substrate II is 0.25 mm; and the thickness of substrate III is 2 mm. Two probes are respectively connected to two patches, forming two L-shaped probe structures. One L-shaped probe structure consists of patch 1 located on the upper surface of substrate II and probe 1. The other L-shaped probe structure consists of patch 2 located on the upper surface of substrate III and probe 2. The middle sections of patch 1 and patch 2 both have a narrower width, and each patch is loaded with a U-shaped slot. Because patch 1 and patch 2 are located on substrates at different heights, the two patches have different widths to reduce the differences in radiative performance for horizontal polarization and vertical polarization. In order to prevent the protruding weld joint after welding the probe from introducing an air gap between substrate I and substrate II to affect the thickness of the antenna, substrates I and II are provided with via holes of diameter D. The patch length in a 2×2 square patches array is W_p, and the gap width between the patches is g. The patches are located on the upper surface of substrate I, and the ground plane is on the lower surface of substrate III. Table 1 lists all the geometrical parameters of the proposed antenna.

2.2. Characteristic Mode Analysis of the Antenna

The modes of the antenna can be explained by CMA [20, 21]. In this design, CMA is used to identify the potential radiation modes of the antenna and guide the improvement of the antenna structure. In the theory of characteristic modes, any induced current $\mathbf{J}$ can be decomposed into multiple weighted characteristic currents, which can be represented as

$$\mathbf{J} = \sum_{n=1}^{N} \alpha_n \mathbf{J}_n \tag{1}$$

Among them, mode weighting coefficient α_n represents the contribution of the modal current $\mathbf{J}_n$ to the total induced current

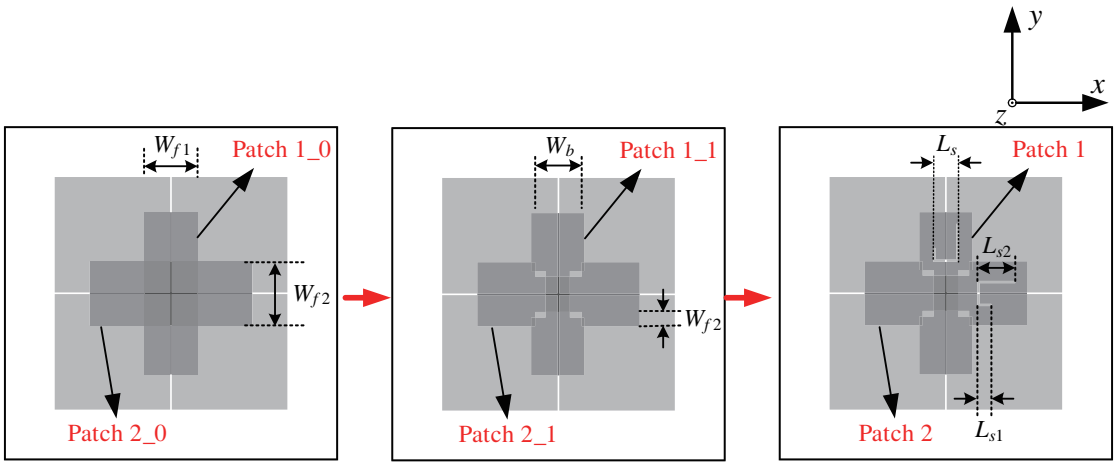

FIGURE 2. Evolution process of patch 1 and patch 2.

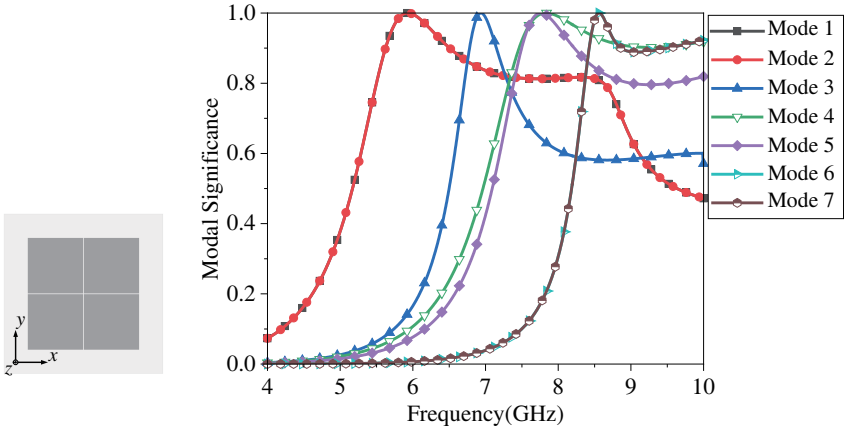

FIGURE 3. The MS for the first seven modes of the 2×2 arrayed patches.

J of the antenna, showing the excitation degree, which can be expressed as

$$\alpha_n = 1/\left(1 + j\lambda_n\right) \int \mathbf{J}_n \cdot \mathbf{E}_i dS \tag{2}$$

where λ_n represents the eigenvalue of the nth mode, $\mathbf{E}_i$ the impressed E-field, and S the surface area of the conductor. The amplitude in the front part of the right side of (2) is referred to as the modal significance (MS), which can be expressed as follows:

$$\text{MS} = 1/\left|1 + j\lambda_n\right| \tag{3}$$

When MS $= 1$, i.e., $\lambda_n = 0$, the corresponding nth mode is in resonance, and the radiation efficiency is highest. The latter part of the right side of (2) is called modal excitation coefficient V_i, which can be expressed as follows:

$$V_i = \int \mathbf{J}_n \cdot \mathbf{E}_i dS \tag{4}$$

Equation (4) shows the relationship between the characteristic current and the external excitation, and a large value indicates a good excitation effect for the antenna.

The evolution process of antenna patch 1 and patch 2 as proposed is illustrated in Figure 2. Figure 3 presents the MS curves for the first seven modes of the 2×2 arrayed patches, and Figure 4 shows the MS curves for the array patches and patch 1_0 and patch 2_0. Among them, Mode 1 and Mode 2 in Figure 3 correspond to Mode 7 and Mode 8 in Figure 4; Modes $3 \sim 5$ in Figure 3 correspond to Modes $3 \sim 5$ in Figure 4; and Mode 6 and Mode 7 in Figure 3 correspond to Mode 11 and Mode 12 in Figure 4. It can be observed that the addition of patch 1_0 and patch 2_0 introduces two linear polarization modes at low frequencies, namely Mode 1 and Mode 2 in Figure 4. Furthermore, the resonant points of Mode 7 and Mode 8 in Figure 4 are significantly influenced by patch 1_0 and patch 2_0, while the resonant points of Modes $3 \sim 5$ are less affected by patch 1_0 and patch 2_0.

As shown in Figure 5, it can be seen that the modal currents of $\mathbf{J}_1$, $\mathbf{J}_2$, $\mathbf{J}_7$, $\mathbf{J}_8$, $\mathbf{J}_{11}$, and $\mathbf{J}_{12}$ are strong on patch 1_0 and patch 2_0, and the current directions are consistent. Therefore, these modes are easily excited by the probe. Other modes are not easily excited or out of the considered frequency band, so their influence can be ignored. As shown in Figure 6, for $\mathbf{J}_1$, $\mathbf{J}_2$, $\mathbf{J}_7$, and $\mathbf{J}_8$, with patch 1_0 and patch 2_0, the direction of modal current on the 2×2 arrayed patches exhibits consistency and good far-field directivity, which satisfies the design requirement of linear polarization mode. The MS curves of $\mathbf{J}_1$ and $\mathbf{J}_2$, and $\mathbf{J}_7$ and $\mathbf{J}_8$ are relatively close, and the modal currents of $\mathbf{J}_1$ and $\mathbf{J}_7$ are concentrated on patch 1_0, while those of $\mathbf{J}_2$

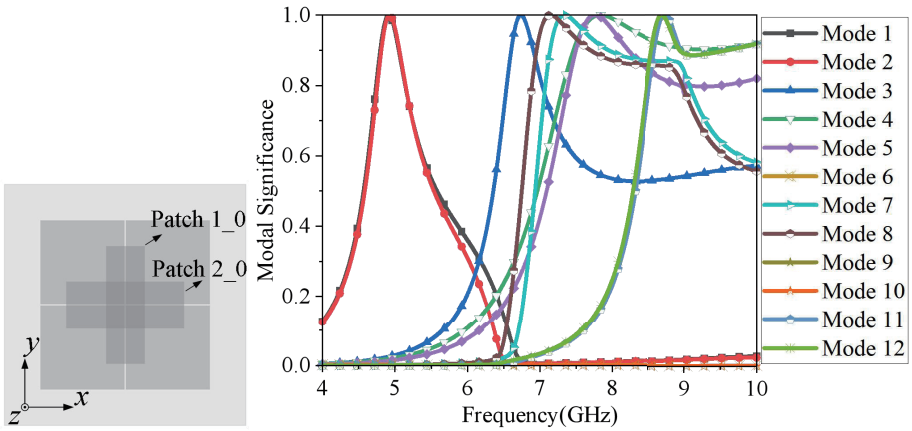

FIGURE 4. MS of the first 12 modes of the 2 × 2 arrayed patches, patch 1_0 and patch 2_0.

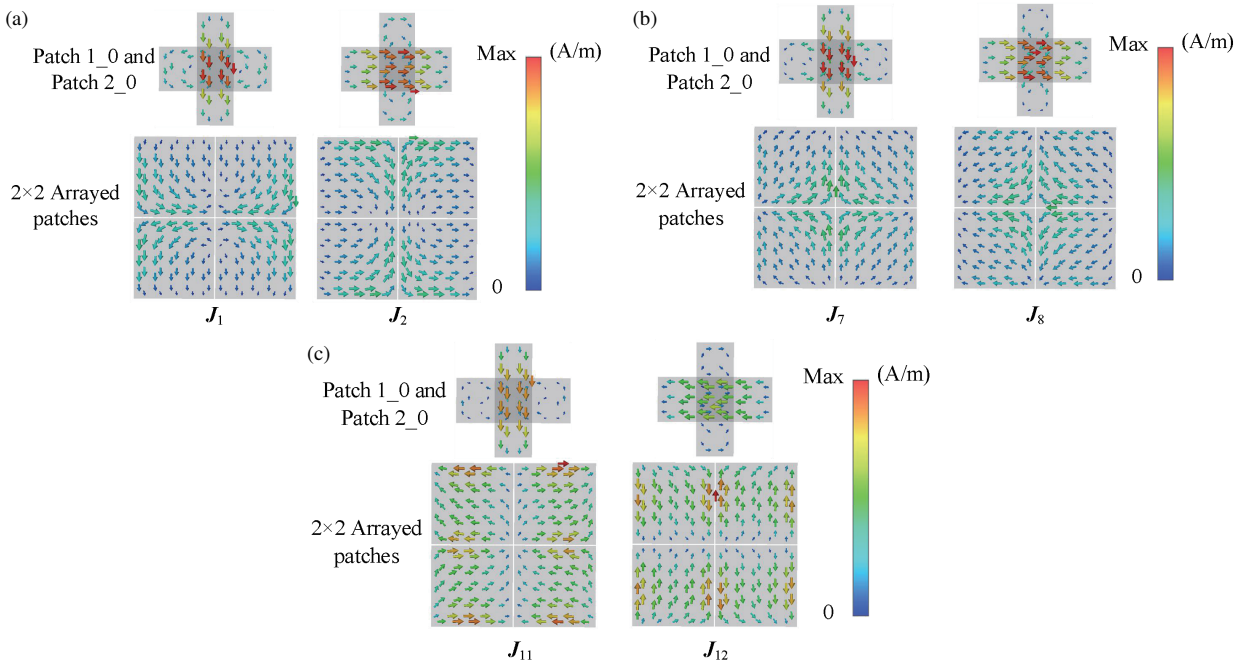

FIGURE 5. Six modal currents that can be excited by the probe. (a) $\mathbf{J}_1$ and $\mathbf{J}_2$ (at 4.9 GHz). (b) $\mathbf{J}_7$ and $\mathbf{J}_8$ (at 7.2 GHz). (c) $\mathbf{J}_{11}$ and $\mathbf{J}_{12}$ (at 8.7 GHz).

and $\mathbf{J}_8$ are concentrated on patch 2_0. Therefore, it is easy to excite $\mathbf{J}_1$ and $\mathbf{J}_7$ by port 1, $\mathbf{J}_2$ and $\mathbf{J}_8$ by port 2, thereby realizing a broadband dual-polarization antenna. For $\mathbf{J}_{11}$ and $\mathbf{J}_{12}$, the directions of modal current on the 2 × 2 arrayed patches are not consistent, resulting in four radiation lobes, which are unwanted high-order modes. However, as shown in Figure 4 for the MS curve, $\mathbf{J}_{11}$ and $\mathbf{J}_{12}$ are easily excited in the same frequency band as $\mathbf{J}_7$ and $\mathbf{J}_8$, which may cause performance degradation such as total radiation pattern. Therefore, it is necessary to ensure that the operational frequency band of $\mathbf{J}_7$ and $\mathbf{J}_8$ is far away from that of $\mathbf{J}_{11}$ and $\mathbf{J}_{12}$.

As shown in Figure 5, the modal currents of $\mathbf{J}_{11}$ and $\mathbf{J}_{12}$ are mainly concentrated on the 2 × 2 arrayed patches, while the modal currents of $\mathbf{J}_1$, $\mathbf{J}_2$, $\mathbf{J}_7$, and $\mathbf{J}_8$ are mainly concentrated on patch 1_0 or patch 2_0. Therefore, changing the structure of patch 1_0 and patch 2_0 has a greater impact on $\mathbf{J}_1$, $\mathbf{J}_2$, $\mathbf{J}_7$, and $\mathbf{J}_8$, and a smaller impact on $\mathbf{J}_{11}$ and $\mathbf{J}_{12}$. Due to the strongest modal currents for $\mathbf{J}_1$, $\mathbf{J}_2$, $\mathbf{J}_7$, and $\mathbf{J}_8$ in the middle of the patch, patch 1_0 and patch 2_0 are chosen to have their middle patch width reduced resulting in patch 1_1 and patch 2_1, in order to position the operating bandwidths of $\mathbf{J}_7$ and $\mathbf{J}_8$ away from those of $\mathbf{J}_{11}$ and $\mathbf{J}_{12}$, as shown in Figure 7.

Figure 7 shows MS curves for the six modes, and Figure 8 shows partial modal currents of the 2 × 2 arrayed patches and patch 1_1 and patch 2_1. It can be seen that after reducing width in middle the resonant frequency points of the MS curves for $\mathbf{J}_1$ and $\mathbf{J}_2$ are shifted to lower frequencies by 0.6 GHz, $\mathbf{J}_7$ and $\mathbf{J}_8$ are shifted to lower frequencies by 1.2 GHz, and $\mathbf{J}_{11}$ and $\mathbf{J}_{12}$ are shifted to lower frequencies by 0.2 GHz.

The MS curves of $\mathbf{J}_{11}$ and $\mathbf{J}_{12}$ are shifted little, so they are almost separated from the operating frequency band of $\mathbf{J}_7$ and $\mathbf{J}_8$. It can be seen from Figure 9 that the radiation directivity of

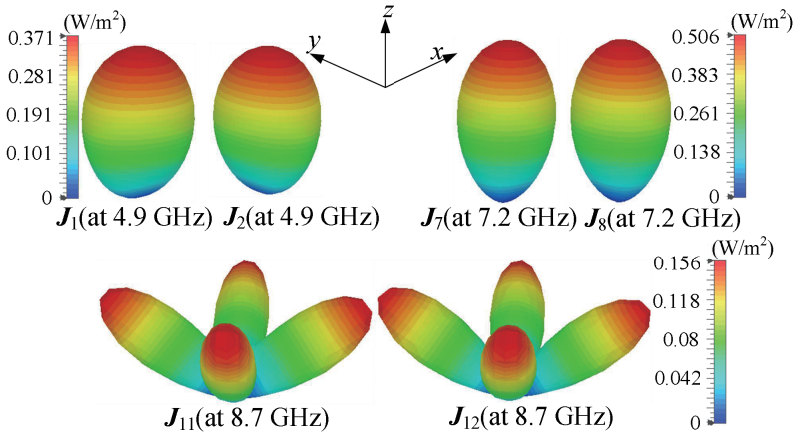

FIGURE 6. Modal radiation patterns for the 2 × 2 arrayed patches, patch 1_0 and patch 2_0.

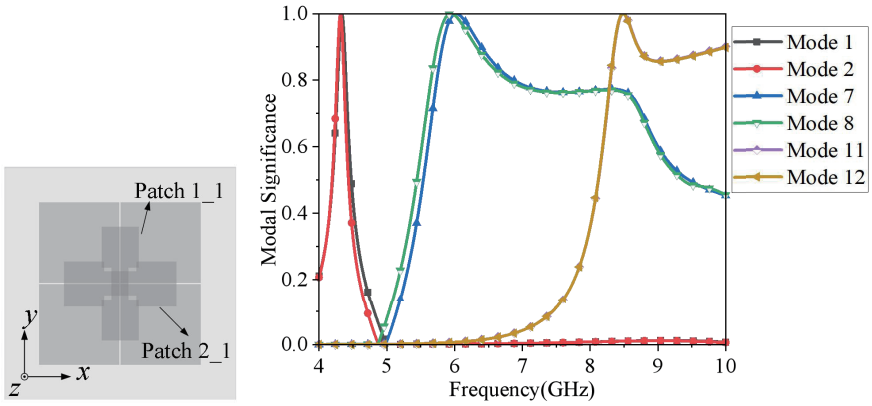

FIGURE 7. Six modes of MS for the 2 × 2 arrayed patches, patch 1_1 and patch 2_1.

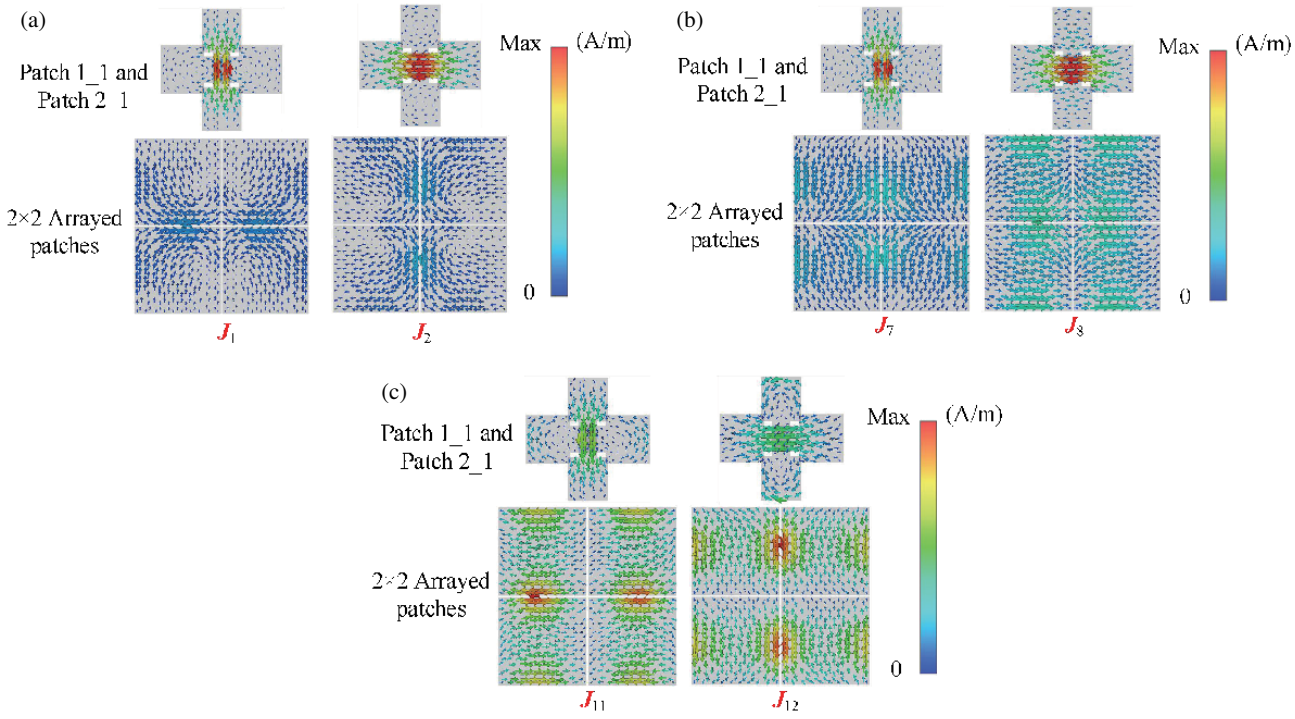

FIGURE 8. Six modal currents that can be excited by the probe. (a)$\mathbf{J}_1$ and $\mathbf{J}_2$ (at 4.3 GHz). (b) $\mathbf{J}_7$ and $\mathbf{J}_8$ (at 6 GHz). (c) $\mathbf{J}_{11}$ and $\mathbf{J}_{12}$ (at 8.5 GHz).

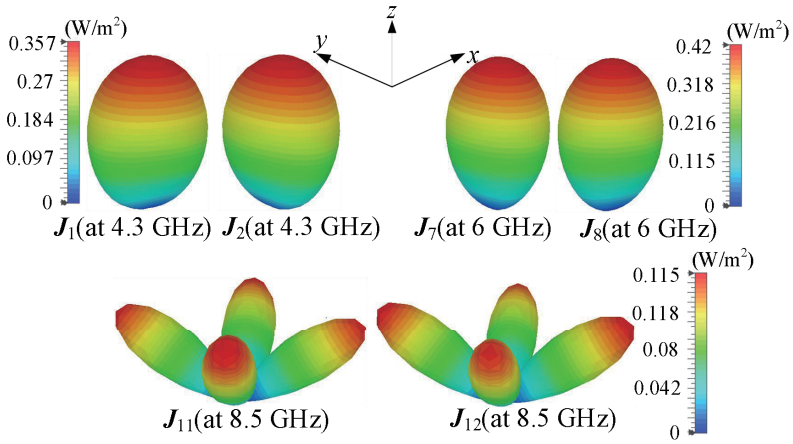

FIGURE 9. Modal radiation patterns for the 2 × 2 arrayed patches, patch 1_1 and patch 2_1.

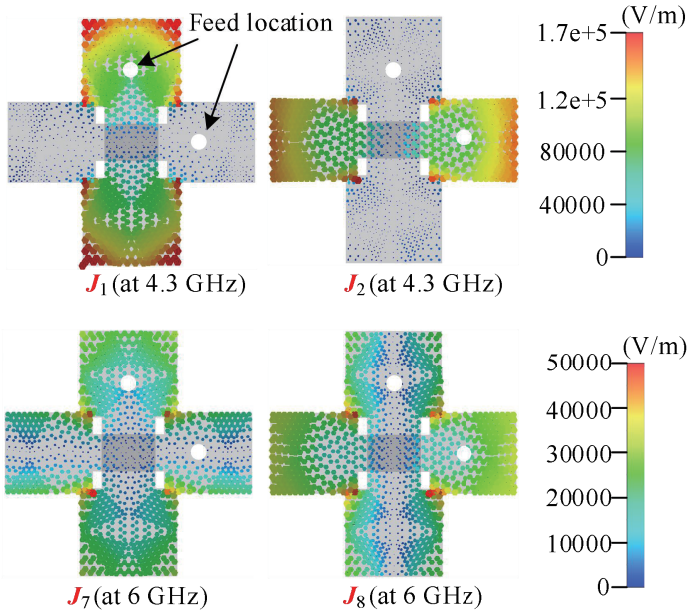

FIGURE 10. Mode electric field distribution on patch 1_1 and patch 2_1.

each mode is not affected by the reduced width in patch middle. It is noted that the mode analysis here does not consider the influence of the excitation and probe, so there would be some deviation for the actual operating frequency bandwidth after adding the excitation and probes.

2.3. Analysis of the Feed Location

Since the L-shaped probe structure is a capacitive coupling feed, it needs to be fed at the point of maximum electric field strength in order to excite the required mode to the fullest extent possible. Therefore, according to the mode electric field distribution on patch 1_1 and patch 2_1 in Figure 10, a probe structure should be added near the location of maximum electric field strength to maximally stimulate the four-line polarized radiation modes of the antenna. As shown in Figure 11, as the size of the probe feeding position Rf increases, its impedance bandwidth gradually increases and then decreases again. When $R_f = 3.15$ mm, the impedance bandwidth is the widest. Therefore, $R_f = 3.15$ mm is chosen to achieve broadband performance.

2.4. Isolation Analysis of the Antenna

Figure 12 shows the variation of S-parameters of the antenna with the reduced width L_b when the U-shaped slots are not loaded. It can be seen that the first resonant frequency point of $|S_{11}|$ is produced by $\mathbf{J}_1$, while the second resonant frequency point is produced by $\mathbf{J}_7$. The second resonant frequency point of the $|S_{11}|$ decreases as the width L_b increases, which is consistent with the MS curve changes shown in Figure 4 and Figure 7.

According to the modal current distribution shown in Figure 8, the strongest modal current of $\mathbf{J}_1$, $\mathbf{J}_2$, $\mathbf{J}_7$, and $\mathbf{J}_8$ are in the middle of patch 1_1 and patch 2_1. At this position, the distance between the two patches is small, resulting in strong cou-

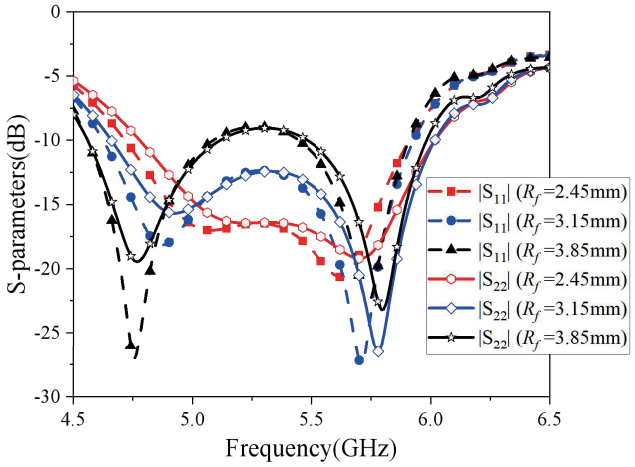

FIGURE 11. The probe feeding position influence of antenna on $|S_{11}|$ and $|S_{22}|$.

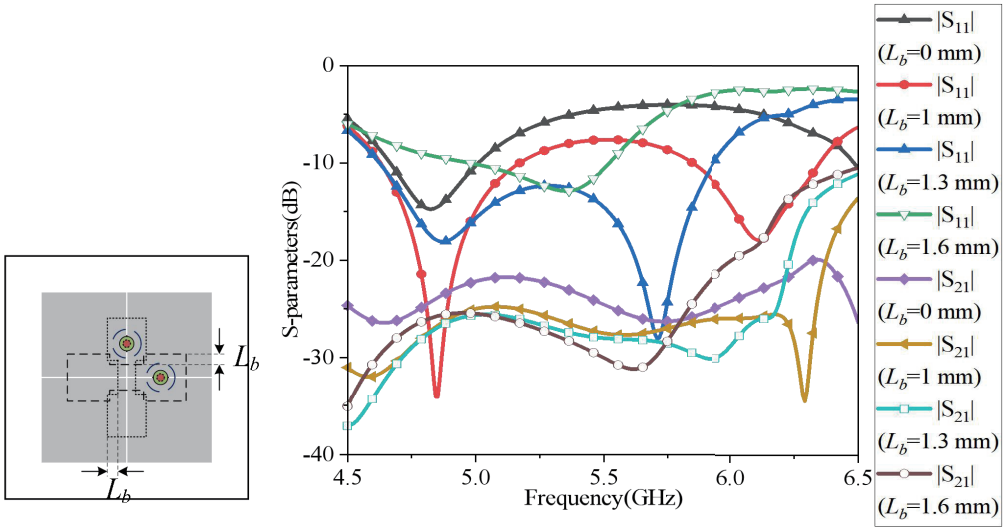

FIGURE 12. The effect of different reduced widths L_b on the S-parameter.

TABLE 2. Comparison of the proposed antenna with reported typical dual-polarized antennas.

Ref.	Center Frequency (GHz)	Relative Size	-10 dB Bandwidth	Port Isolation (dB)	FBRs (dB)	cross-polarization Level (dB)
[1]	2.4	$0.81\lambda_0 \times 0.81\lambda_0 \times 0.088\lambda_0$	18.8%	> 28.5	> 15	-20
[7]	5.5	$1.15\lambda_0 \times 1.15\lambda_0 \times 0.067\lambda_0$	25.5%	> 34.0	> 10	-28
[12]	1.9	$1.94\lambda_0 \times 1.94\lambda_0 \times 0.15\lambda_0$	28.9%	> 33	> 15	-15
[18]	2.6	$0.57\lambda_0 \times 0.57\lambda_0 \times 0.062\lambda_0$	10.0%	> 20	> 14	-25
[21]	5.49	$0.55\lambda_0 \times 0.55\lambda_0 \times 0.096\lambda_0$	18.6%	> 16	> 20	-15
This Work	5.4	$0.54\lambda_0 \times 0.54\lambda_0 \times 0.068\lambda_0$	23.5%	> 27.9	> 22	-23

pling. This means that reducing middle width on the patches can reduce this area to reduce coupling and improve isolation between ports, which can be seen from Figure 12 where $|S_{21}|$ decreases with increasing L_b.

In order to further increase the isolation, U-shaped slots with the same dimensions are etched on patch 1 and patch 2 with the reduced middle width, as shown in Figure 1. From Figure 13, it is evident that the loading of the U-shaped slots directs the mode current to flow along the edges of the slots, resulting in a relative attenuation of the mode current near the probe's feed position compared to Figure 8. Figure 14 shows the surface current distribution on probe 1, patch 1_1, patch 2_1, patch 1,

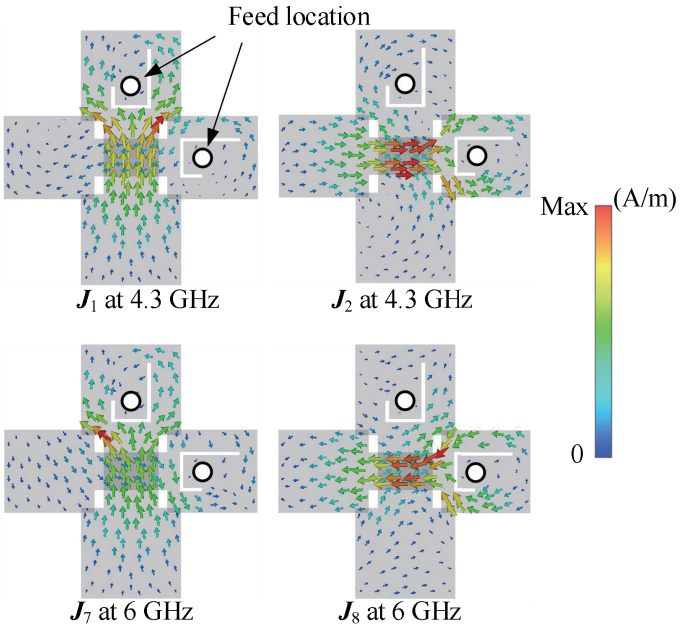

FIGURE 13. Mode currents distribution on patch 1 and patch 2.

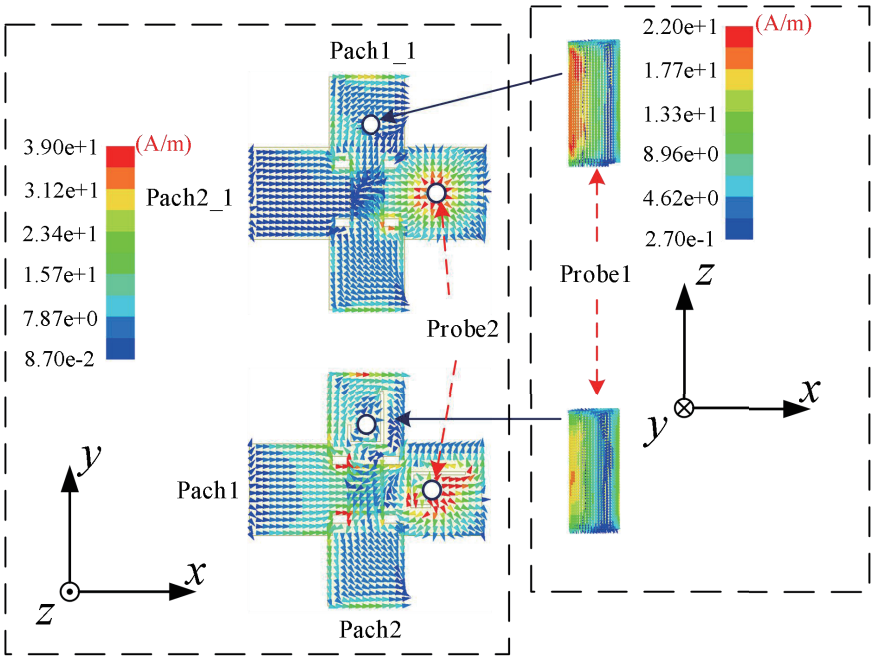

FIGURE 14. Comparison of current distribution on patch 1_1, patch 2_1, and patch 1 and patch 2.

and patch 2 when probe 2 is fed at 5.5 GHz. It can be observed that the loading U-shaped slots cause surface currents to flow along the edges of the slots, weakening the coupled current on the probe to increase isolation. Therefore, the U-shaped slots have the effect of increasing isolation between ports.

Figure 15 shows the impact of the loaded U-shaped slots on the S-parameters of the antenna. It can be seen that the loaded U-shaped slots have a small impact on the operating frequency bandwidth of the antenna. At the same time, it can be observed that the maximum value of $|S_{21}|$ of the antenna is decreased from -25 dB without U-shaped slots to -31 dB with U-shaped slots, indicating a significant increase in isolation. So, from the S-parameter, it is confirmed that the role of U-shaped slots is to improve the isolation.

3. SIMULATED AND MEASURED RESULTS

Figure 16 shows the fabricated antenna with an overall size of 30 mm $\times$ 30 mm $\times$ 3.75 mm ($0.54\lambda_0 \times 0.54\lambda_0 \times 0.068\lambda_0$, λ_0 is the free-space wavelength of central frequency). Figure 17(a) compares the simulated and measured S-parameters

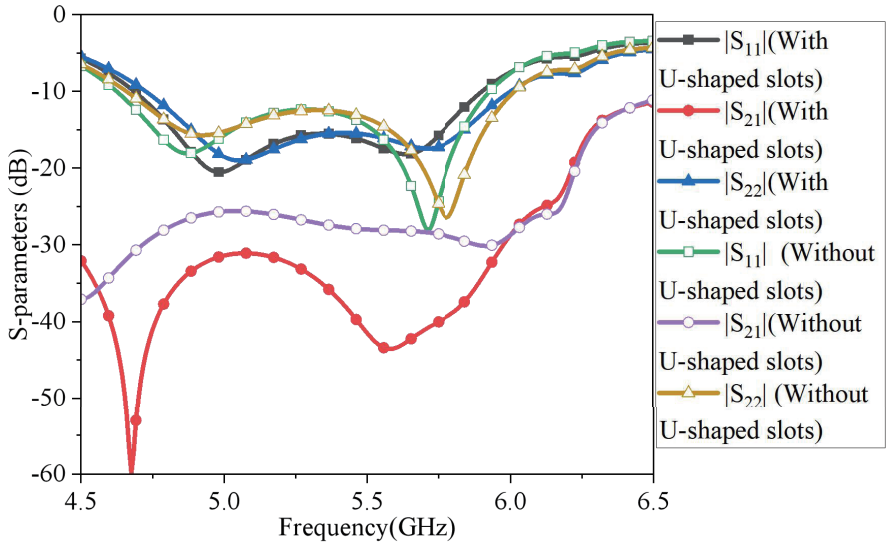

FIGURE 15. S-parameters of the proposed antenna with and without U-shaped slots.

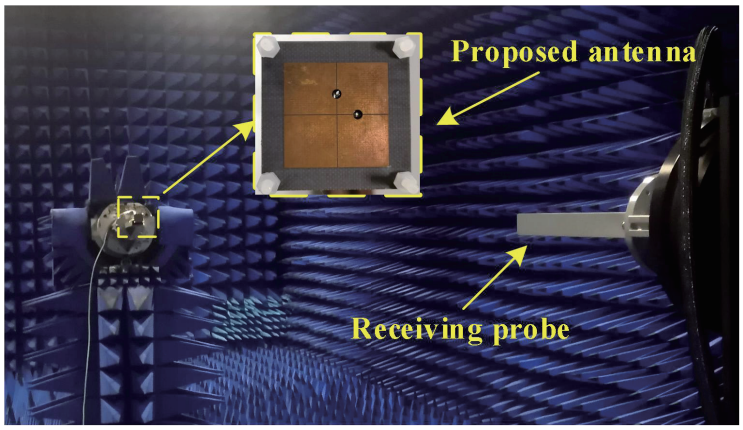

FIGURE 16. Photograph of the proposed antenna and far-field measurement environment.

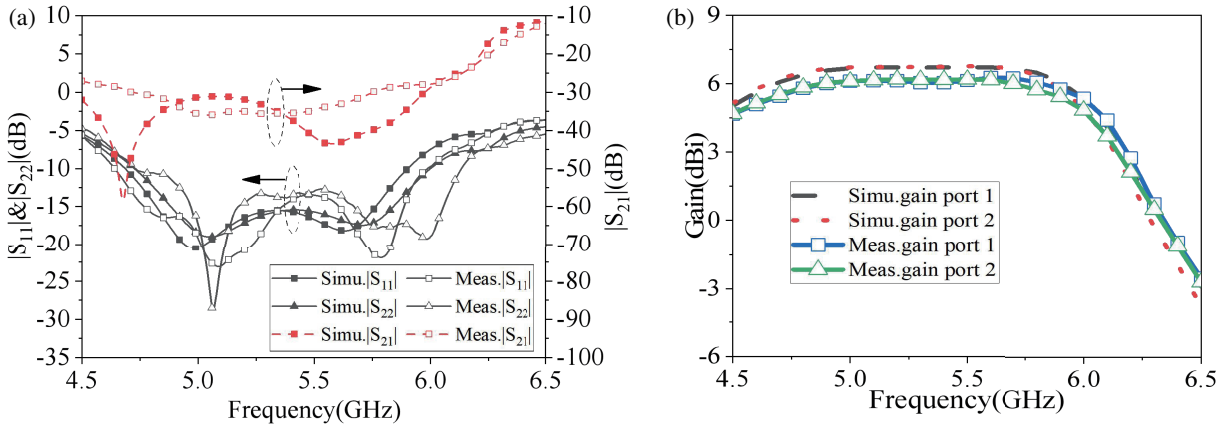

FIGURE 17. Simulated and measured results. (a) S-parameters. (b) Gains.

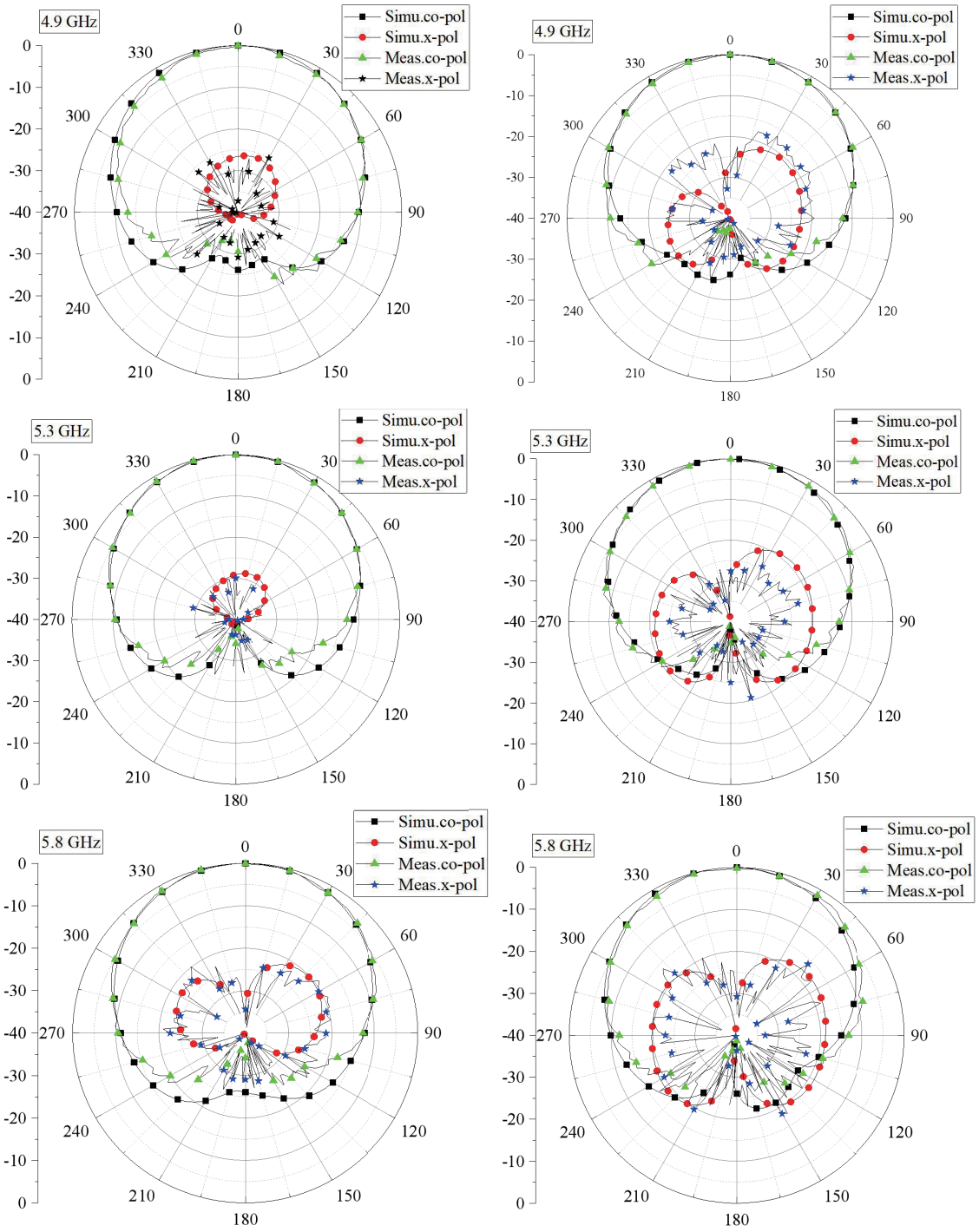

FIGURE 18. The E-plane (left) and the H-plane (right) radiation patterns excited by Port 1.

of the antenna and shows good consistency between simulated and measured results. The antenna has a measured −10 dB impedance bandwidth of 4.73–5.99 GHz (23.5%) for dual polarizations. Within this range, an isolation level exceeding 27.9 dB was measured, showcasing high isolation performance that facilitates achieving superior signal-to-noise ratio and channel capacity for the communication system. As shown in Figure 17(b), the gain changes for dual polarizations within the −10 dB impedance bandwidth range are within 4.8–6.2 dBi. The difference in gain between the simulated and measured results is less than 0.8 dB, which may be due to the misalignment between the proposed antenna as the transmitting antenna and receiving probe, as well as manufacturing errors.

Figures 18 and 19 show the simulated and measured radiation patterns when port 1 and port 2 are excited, respectively. The simulated and measured results are in good agreement. It can be seen that FBRs of the antenna obtained by measurements are greater than 22 dB when port 1 or port 2 is excited within

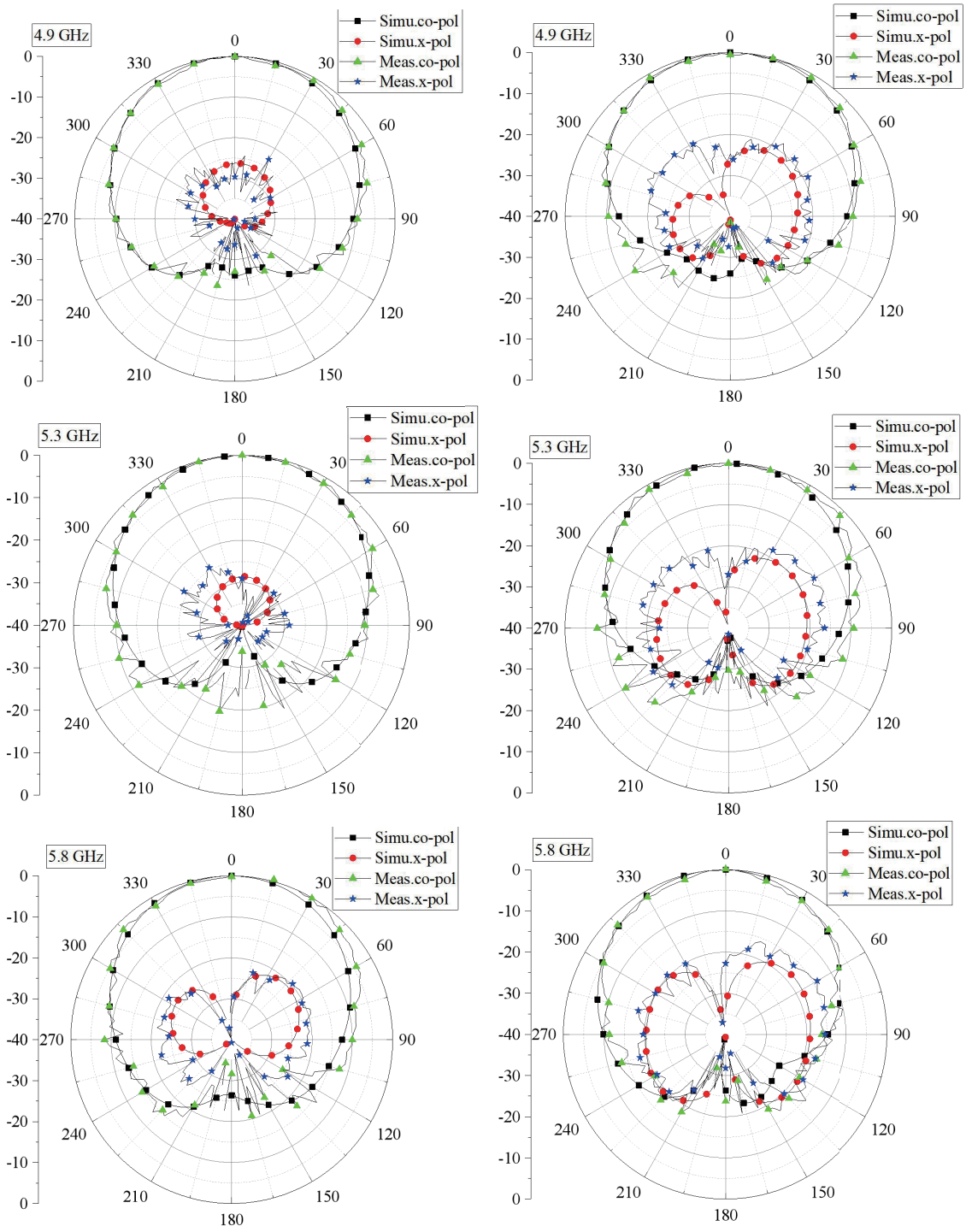

FIGURE 19. The E-plane (left) and the H-plane (right) radiation patterns excited by Port 2.

the operating frequency band. Within the operating frequency band, the cross-polarization levels obtained by measurements are less than -23 dB. Within the operating frequency band, the E-plane half-power beamwidths (HPBWs) measured at Port 1 and Port 2 are $81° \pm 3°$ and $92° \pm 10°$, respectively. The H-plane HPBWs are $84° \pm 3°$ and $80° \pm 5°$. The antenna has a stable radiation pattern over the entire operating frequency range.

The proposed antenna is compared with several typical dual-polarized antennas as listed in Table 2. Compared to the dual-polarized antennas with feeding network [1, 7, 12], the proposed antenna not only has a smaller size but also has higher FBRs. Compared to the compact dual-polarized antennas with probe feed [18, 21], the proposed antenna has a wider operating bandwidth and higher isolation. It can be seen that the proposed antenna demonstrates a compact size along with a wide band-

width, high isolation, low cross-polarization levels, and high FBRs.

4. CONCLUSIONS

In this paper, a compact wideband high-isolation dual-polarized antenna is proposed. The compactness of the antenna is achieved by using two closely spaced L-shaped probe structures. CMA is used to explain the radiation pattern of the antenna and improve its structure. The proposed antenna is fabricated and measured for validation. The measured results show that the proposed antenna has a 23.5% bandwidth (4.73–5.99 GHz) and 27.9 dB port isolation. Moreover, the antenna has FBRs greater than 22 dB and cross-polarization levels less than −23 dB. Therefore, the proposed antenna has a compact size and good performance, which has potential application value in wireless communication systems with limited space such as WiFi and arrays.

ACKNOWLEDGEMENT

This work was supported by the Scientific and Technological Research Program of Chongqing Municipal Education Commission (KJQN202300611), Chongqing Postgraduate Research and Innovation Project (CYS22445).

REFERENCES

[1] Deng, C., Y. Li, Z. Zhang, and Z. Feng, "A wideband high-isolated dual-polarized patch antenna using two different balun feedings," *IEEE Antennas and Wireless Propagation Letters*, Vol. 13, 1617–1619, 2014.

[2] Sun, F., Y. Li, J. Wang, Y. Ma, L. Ge, B. Ai, and R. He, "A millimeter-wave wideband dual-polarized antenna array with 3-D-printed air-filled differential feeding cavities," *IEEE Transactions on Antennas and Propagation*, Vol. 70, No. 2, 1020–1032, Feb. 2022.

[3] Feng, B., H. Li, K. L. Chung, L. Deng, C.-Y.-D. Sim, and L. Deng, "A dual-polarized wideband ceiling-mount antenna with low gain variations and high isolation for 5G Sub-6 GHz applications," *IEEE Transactions on Antennas and Propagation*, Vol. 70, No. 9, 8572–8577, Sep. 2022.

[4] Tang, X., H. Chen, B. Yu, W. Che, and Q. Xue, "Bandwidth enhancement of a compact dual-polarized antenna for sub-6G 5G CPE," *IEEE Antennas and Wireless Propagation Letters*, Vol. 21, No. 10, 2015–2019, Oct. 2022.

[5] Zhang, H., D. Ding, and X. Y. Zhang, "Broadband dual-polarized antenna with stable radiation patterns for base station applications," *IEEE Antennas and Wireless Propagation Letters*, Vol. 22, No. 2, 337–341, Feb. 2023.

[6] Le Thi, C. H., S. X. Ta, X. Q. Nguyen, K. K. Nguyen, and C. Dao-Ngoc, "Design of compact broadband dual-polarized antenna for 5G applications," *International Journal of RF and Microwave Computer-Aided Engineering*, Vol. 31, No. 5, e22615, May 2021.

[7] Lin, F. H. and Z. N. Chen, "Resonant metasurface antennas with resonant apertures: Characteristic mode analysis and dual-polarized broadband low-profile design," *IEEE Transactions on Antennas and Propagation*, Vol. 69, No. 6, 3512–3516, Jun. 2021.

[8] Wang, J., W. Wang, A. Liu, M. Guo, and Z. Wei, "Miniaturized dual-polarized metasurface antenna with high isolation," *IEEE Antennas and Wireless Propagation Letters*, Vol. 20, No. 3, 337–341, Mar. 2021.

[9] Wang, J., W. Wang, A. Liu, M. Guo, and Z. Wei, "Broadband metamaterial-based dual-polarized patch antenna with high isolation and low cross polarization," *IEEE Transactions on Antennas and Propagation*, Vol. 69, No. 11, 7941–7946, Nov. 2021.

[10] Liu, S., D. Yang, Y. Chen, X. Zhang, and Y. Xiang, "High isolation and low cross-polarization of low-profile dual-polarized antennas via metasurface mode optimization," *IEEE Transactions on Antennas and Propagation*, Vol. 69, No. 5, 2999–3004, May 2021.

[11] Wong, H., K.-L. Lau, and K.-M. Luk, "Design of dual-polarized L-probe patch antenna arrays with high isolation," *IEEE Transactions on Antennas and Propagation*, Vol. 52, No. 1, 45–52, Jan. 2004.

[12] Guo, Y.-X., K.-W. Khoo, and L. C. Ong, "Wideband dual-polarized patch antenna with broadband baluns," *IEEE Transactions on Antennas and Propagation*, Vol. 55, No. 1, 78–83, Jan. 2007.

[13] Ryu, K. S. and A. A. Kishk, "Wideband dual-polarized microstrip patch excited by hook shaped probes," *IEEE Transactions on Antennas and Propagation*, Vol. 56, No. 12, 3645–3649, Dec. 2008.

[14] Jin, Y. and Z. Du, "Broadband dual-polarized F-probe fed stacked patch antenna for base stations," *IEEE Antennas and Wireless Propagation Letters*, Vol. 14, 1121–1124, 2015.

[15] Qin, X. and Y. Li, "Compact dual-polarized cross-slot antenna with colocated feeding," *IEEE Transactions on Antennas and Propagation*, Vol. 67, No. 11, 7139–7143, Nov. 2019.

[16] Gosalia, K. and G. Lazzi, "Reduced size, dual-polarized microstrip patch antenna for wireless communications," *IEEE Transactions on Antennas and Propagation*, Vol. 51, No. 9, 2182–2186, Sep. 2003.

[17] He, Y. and Y. Li, "Dual-polarized microstrip antennas with capacitive via fence for wide beamwidth and high isolation," *IEEE Transactions on Antennas and Propagation*, Vol. 68, No. 7, 5095–5103, Jul. 2020.

[18] Gou, Y., S. Yang, Q. Zhu, and Z. Nie, "A compact dual-polarized double E-shaped patch antenna with high isolation," *IEEE Transactions on Antennas and Propagation*, Vol. 61, No. 8, 4349–4353, Aug. 2013.

[19] Kim, G. and S. Kim, "Design and analysis of dual polarized broadband microstrip patch antenna for 5G mmWave antenna module on FR4 substrate," *IEEE Access*, Vol. 9, 64 306–64 316, 2021.

[20] Lin, F. H. and Z. N. Chen, "Low-profile wideband metasurface antennas using characteristic mode analysis," *IEEE Transactions on Antennas and Propagation*, Vol. 65, No. 4, 1706–1713, Apr. 2017.

[21] Zhang, S., X.-S. Yang, B.-J. Chen, and B.-Z. Wang, "Miniaturized wideband ±45° dual-polarized metasurface antenna by loading quasi-fractal slot," *IEEE Antennas and Wireless Propagation Letters*, Vol. 22, No. 4, 893–897, Apr. 2023.